Journal of Sound and Vibration (1999) **219**(1), 133–155
Article No. jsvi.1998.1823, available online at http://www.idealibrary.com.on IDEAL

TRANSVERSE MODE LOCALIZATION IN A DUAL-SPAN ROTATING SHAFT

B. KANG AND C. A. TAN

Department of Mechanical Engineering, Wayne State University, Detroit, MI 48202, *U.S.A.*

(*Received* 26 *January* 1998, *and in final form* 3 *August* 1998)

In this paper, transverse mode localization in a dual-span rotating shaft is studied. The shaft is elastically supported by transverse and rotational springs at an intermediate point and at both ends. A Timoshenko beam model including the effects of axial loads is employed, and a small disorder in the span length is introduced in the study of the mode localization. The exact eigensolutions of the systems are obtained by the phase closure principle. Based on actual values of typical bearing stiffness applied in turbo machinery, the effects of support stiffness, rotation speed and axial load on the mode localization are examined. These results are compared with those obtained from the Rayleigh shaft model to assess the effects of shear deformation. It is shown that mode localization depends strongly on the modelling of the bearing support.

1. INTRODUCTION

Flexible shaft elements rotating about the longitudinal axis are commonly employed as high speed cutting tools or as a means of power transmission in many engineering applications such as gas or hydraulic turbines, internal combustion engines, and turbo generators. Recent demands on the performance of these machine elements at severe operating conditions and the applications of lighter components require the use of more reliable, failure-safe elements and more accurate models for analysis. Three beam theories, the Euler–Bernoulli, Rayleigh and Timoshenko models, have been proposed to study the vibration of rotating shafts. As more accurate analyses are required, it is recognized that the Timoshenko theory, which includes both the effects of rotary inertia and shear deformation, should be used to accurately predict the natural frequencies and vibration modes of stubby beams [1].

Numerous studies on the vibrations of rotating shafts are well documented [2–5]. One of the most important topics is the study of the effects of critical parameters such as end loads, bearing stiffness and overhang mass on the stability and critical speeds of rotating shafts [6–8]. Other studies focus on the development of solution techniques to investigate the dynamic response and vibration of

0022–460X/99/010133 + 23 $30.00/0

different rotating shaft models. A model of a rotating Timoshenko shaft subjected to axial loads was proposed by applying a finite strain beam theory and Hamilton's Principle [9]. The transient response of rotating Rayleigh and Timoshenko shafts was evaluated by a finite integral transform [10] and a modal analysis technique [11], respectively. Exact solutions for the free and forced responses of a stepped, rotating Timoshenko shaft system were obtained by the distributed transfer function method and a generalized displacement formulation [12]. Using the axially strained, rotating Timoshenko shaft model of reference [9], the reflection and transmission characteristics of waves incident upon an arbitrary support or discontinuity were presented [13].

Although there has been much research on the dynamics and vibration of rotating shafts, the dynamics of rotating multi-span shafts with structural disorder has not been considered. In many engineering applications, a rotating shaft is supported by multiple bearings. In particular, when the bearings with identical stiffness are equally spaced along the shaft, the rotating shaft becomes periodic with sub-spans inter-coupled by elastic constraints on either or both the transverse and rotational motions. Hodges introduced the *confinement of vibration* or *normal mode localization* in which vibration amplitudes are confined to some sub-spans as a result of structural irregularity in periodic mechanical structures [14]. Thus, with reference to the context of mode localization, transverse vibration modes of a multi-span rotating shaft can be strongly localized when the span lengths are slightly disordered, either by error or design.

Since the work of Hodges, there has been extensive research on the dynamics and vibrations of disordered periodic and cyclically symmetric structures. Here we cite work on linear systems only. Hodges and Woodhouse, in a supplementary study on normal mode localization by both theory and experiment, formulated the *localization factor* which gives the average spatial decay rate of vibration amplitude [15]. Valero and Bendiksen [16], and Bendiksen [17] studied the mode localization behaviour in weakly coupled cyclically symmetric systems such as mistuned turbomachinery blades and wrap-rip disk antenna. Pierre *et al*. [18] applied a modified perturbation method to study mode localization and also experimentally verified the existence of localized modes for a disordered dual-span Euler–Bernoulli beam model. Pierre [19] and Chen and Ginsberg [20] investigated the relationship between mode localization and eigenvalue loci veering of nearly periodic structures by applying a perturbation method to a general eigenvalue problem and found that small disorder results in a strong mode localization in the eigenvalue veering zone. It was also concluded that occurrence of eigenvalue veering indicated a *directional vibration localization* which could be present in axisymmetric structures with some type of irregularities breaking the symmetry [19]. For example, Ulsoy *et al*. [21, 22] demonstrated that vibration modes could be localized in one of the two orthogonal principal directions of a single-span, rotating Rayleigh shaft with non-circular cross-sections. Other studies of mode localization include band-wheel systems [23] and axially moving beams [24–26]. One general conclusion from all these studies is that the degree of mode localization depends on the ratio of the disorder strength to the coupling strength between adjacent sub-structures.

The purpose of this paper is to investigate the mode localization in a dual-span rotating shaft with an intermediate support. A disorder in the span length is introduced. While most studies have examined beams with a mono-coupling mechanism (simple supports with elastic rotational constraints), a bi-coupling elastic constraint on both the transverse and rotational motions is considered in this work. This constraint models more closely a bearing support. Note that our study is not the first to examine this type of coupling. Lust *et al*. [27] presented a numerical study on the mode localization of a bi-coupled, multi-span Timoshenko beam. In section 2, the problem is formulated, and in section 3, the wave solution approach of reference [13] is applied to obtain the exact eigensolutions. To assess the effects of shear deformation on mode localization, results of the Timoshenko and Rayleigh models are compared. The effects of system parameters such as support stiffness, rotation speed (considering both forward and backward precession modes), and axial load on mode localization are studied in section 4.

2. PROBLEM FORMULATION AND WAVE SOLUTIONS

Figure 1 depicts a rotating shaft with an intermediate elastic support and elastic boundaries. The shaft is subject to axial loads P. Including the effects of rotary inertia, shear deformations, and axial deformations due to the axial loads, the

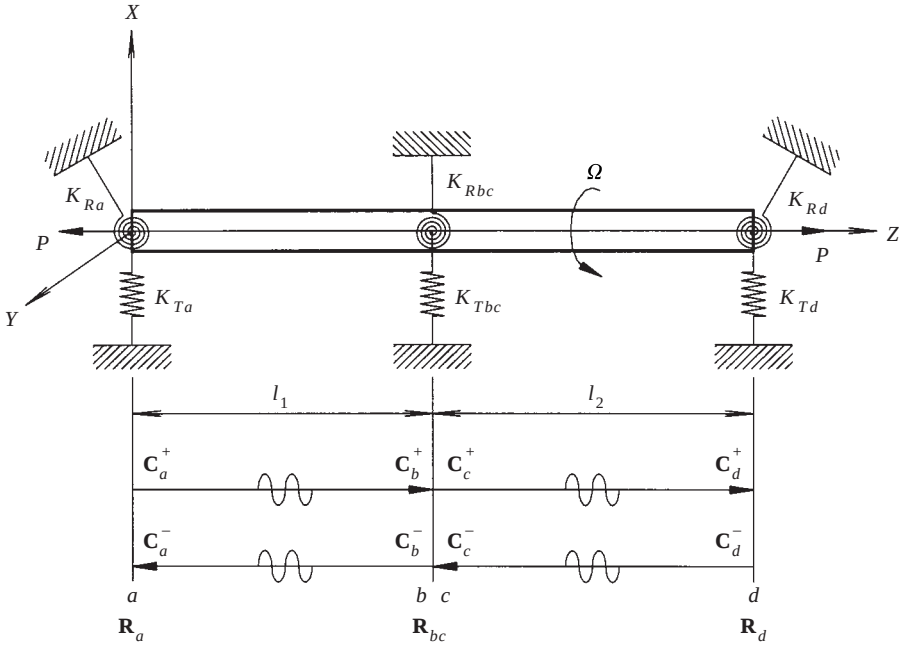

Figure 1. A dual-span shaft, subject to axial loads P and with elastic support boundaries, rotates about its longitudinal axis Z at constant speed Ω.

uncoupled equation of motion governing the transverse displacement U is given in the following non-dimensional form [9]

$$\frac{\partial^4 u}{\partial z^4} - (1+\alpha)\frac{\partial^4 u}{\partial z^2\,\partial t^2} + 2\mathrm{i}\beta\frac{\partial^3 u}{\partial z^2\,\partial t} - 2\mathrm{i}\beta\frac{\partial^3 u}{\partial t^3} + \alpha\frac{\partial^4 u}{\partial t^4} - 16\varepsilon\left(1+\varepsilon-\frac{\varepsilon}{\alpha}\right)\frac{\partial^2 u}{\partial z^2}$$

$$+ 16\alpha(1+\varepsilon)\left(1+\varepsilon-\frac{\varepsilon}{\alpha}\right)\frac{\partial^2 u}{\partial t^2} = 0, \tag{1}$$

where

$$u = \frac{U}{a_0}, \quad z = \frac{Z}{a_0}, \quad t = \frac{T}{T_0}, \quad T_0 = \sqrt{\frac{\rho a_0^2}{KG}}, \quad \alpha = \frac{KG}{E}, \quad \beta = \frac{\rho a_0^2}{ET_0}\Omega, \quad \varepsilon = \frac{P}{EA_s}. \tag{1a}$$

Note that U is the displacement in the complex plane, $U = U_x + \mathrm{i}U_y$, where $\mathrm{i} = \sqrt{-1}$. E denotes the Young's modulus, ρ the mass density, A_s the area of the cross section, a_0 the diameter of the shaft, K the Timoshenko shear coefficient, G the shear modulus and Ω the constant angular velocity of the shaft. In Figure 1, the stations a, b, c, d denote the left boundary, the left and the right of the intermediate support, and the right boundary, respectively. The non-dimensional spring stiffness constants are defined as

$$\text{transverse spring: } k_t = \frac{K_T a_0}{KAG}, \tag{2a}$$

$$\text{rotational spring: } k_r = \frac{K_R a_0}{EI}. \tag{2b}$$

We assume the following harmonic wave solution

$$u(z,t) = C\,\mathrm{e}^{\mathrm{i}(\bar{\gamma}z + \bar{\omega}t)}, \tag{3}$$

and define the non-dimensional wavenumber $\bar{\gamma}$ and frequency $\bar{\omega}$

$$\bar{\gamma} = \gamma a_0, \tag{4a}$$

$$\bar{\omega} = \frac{\omega a_0}{c_s}\left(c_s = \sqrt{\frac{KG}{\rho}} \text{ is known as the } \textit{shear velocity}\right). \tag{4b}$$

Substituting the harmonic wave solution into equation (1) gives the frequency equation

$$\bar{\gamma}^4 - A\bar{\gamma}^2 + B = 0, \tag{5}$$

where

$$A = (1+\alpha)\bar{\omega}^2 - 2\beta\bar{\omega} - 16\varepsilon\left(1+\varepsilon-\frac{\varepsilon}{\alpha}\right), \tag{5a}$$

$$B = \bar{\omega}^2\left[\alpha\bar{\omega}^2 - 2\beta\bar{\omega} - 16\alpha(1+\varepsilon)\left(1+\varepsilon-\frac{\varepsilon}{\alpha}\right)\right]. \tag{5b}$$

In general, the four roots of equation (5) are complex. However, for real $\bar{\omega}$, it can be shown that $A^2 - 4B$ is positive semi-definite for most engineering applications with $\alpha > 0$ and $-1 \leqslant \varepsilon \leqslant 1$. Hence, based on the algebraic relationships between A and B, the Timoshenko shaft model has four distinct wave solutions [13]. In the present paper, only vibration modes below the non-zero cutoff frequency $\bar{\omega}_c$,

$$\bar{\omega} = \frac{\beta}{\alpha} + \sqrt{\left(\frac{\beta}{\alpha}\right)^2 + 16(1+\varepsilon)\left(1+\varepsilon-\frac{\varepsilon}{\alpha}\right)}, \tag{6}$$

are considered, i.e., $B < 0$. Note that for $\beta = 0$ and $\varepsilon = 0$, $\bar{\omega}_c$ is 4 or about 20 kHz which is far beyond the practical range of frequencies. The wave solutions are then

$$u(z,t) = (C_{u1}^{+}\,\mathrm{e}^{-\mathrm{i}\bar{\gamma}_1 z} + C_{u1}^{-}\,\mathrm{e}^{\mathrm{i}\bar{\gamma}_1 z} + C_{u2}^{+}\,\mathrm{e}^{-\bar{\gamma}_2 z} + C_{u2}^{-}\,\mathrm{e}^{-\bar{\gamma}_2 z})\,\mathrm{e}^{\mathrm{i}\bar{\omega}t}, \quad \text{for } A \geqslant 0, \tag{7}$$

$$u(z,t) = (C_{u1}^{+}\,\mathrm{e}^{-\bar{\gamma}_1 z} + C_{u1}^{-}\,\mathrm{e}^{\bar{\gamma}_1 z} + C_{u2}^{+}\,\mathrm{e}^{-\mathrm{i}\bar{\gamma}_2 z} + C_{u2}^{-}\,\mathrm{e}^{\mathrm{i}\bar{\gamma}_2 z})\,\mathrm{e}^{\mathrm{i}\bar{\omega}t}, \quad \text{for } A < 0, \tag{8}$$

where

$$\bar{\gamma}_1 = \frac{1}{\sqrt{2}}(\sqrt{A^2 + 4|B|} + |A|)^{1/2}, \qquad \bar{\gamma}_2 = \frac{1}{\sqrt{2}}(\sqrt{A^2 + 4|B|} - |A|)^{1/2}, \tag{9}$$

and the coefficients C^{+} and C^{-} denote positive- and negative-travelling waves from the origin of disturbance, respectively. Note that both wave solutions (7) and (8) have two propagating and two attenuating wave components.

For comparison of results to be presented later, the parameters A and B for the Rayleigh shaft model neglecting the effects of shear and axial deformation are

$$A = \alpha\bar{\omega}^2 - 2\beta\bar{\omega} - 16\varepsilon, \qquad B = -16\alpha\bar{\omega}^2. \tag{10}$$

For convenience, the overbar on the non-dimensional quantities is dropped hereafter.

3. EIGENSOLUTIONS OF THE SYSTEM

The characteristic equation of the system is obtained by the phase closure principle [28, 29]. Group the wave components into 2×1 vectors of positive- and negative-travelling waves:

$$\mathbf{C}^{+} = \begin{Bmatrix} C_{u1}^{+} \\ C_{u2}^{+} \end{Bmatrix}, \qquad \mathbf{C}^{-} = \begin{Bmatrix} C_{u1}^{-} \\ C_{u2}^{-} \end{Bmatrix}. \tag{11a, b}$$

Referring to Figure 1, the relation between the incident, reflected and transmitted waves are

$$\mathbf{C}_d^{-} = \mathbf{R}_d\mathbf{C}_d^{+}, \qquad \mathbf{R}_d = \mathbf{r}_d, \tag{12a}$$

$$\mathbf{C}_c^{-} = \mathbf{R}_c\mathbf{C}_c^{+}, \qquad \mathbf{R}_c = \mathbf{T}_2\mathbf{r}_d\mathbf{T}_2, \tag{12b}$$

$$\mathbf{C}_b^- = \mathbf{R}_{bc}\mathbf{C}_b^+, \qquad \mathbf{R}_{bc} = \mathbf{r}_{bc} + \mathbf{t}_{bc}(\mathbf{R}_c^{-1} - \mathbf{r}_{bc})^{-1}\mathbf{t}_{bc}, \tag{12c}$$

$$\mathbf{C}_a^- = \mathbf{T}_1\mathbf{C}_b^-, \tag{12d}$$

$$\mathbf{C}_a^+ = \mathbf{R}_a\mathbf{C}_a^-, \qquad \mathbf{R}_a = \mathbf{r}_a, \tag{12e}$$

$$\mathbf{C}_b^+ = \mathbf{T}_1\mathbf{C}_a^+, \tag{12f}$$

where the subscripts denote the locations, $\mathbf{R}$ is a reflection matrix relating the amplitudes of positive- and negative-travelling waves at the support and the boundaries, and $\mathbf{T}_1$ and $\mathbf{T}_2$ are the field transfer matrices defined as

$$\mathbf{T}_1 = \begin{bmatrix} e^{-i\gamma_1(l_1/a_0)} & 0 \\ 0 & e^{-\gamma_2(l_2/a_0)} \end{bmatrix}, \qquad \mathbf{T}_2 = \begin{bmatrix} e^{-i\gamma_1(l_2/a_0)} & 0 \\ 0 & e^{-\gamma_2(l_2/a_0)} \end{bmatrix}, \quad \text{for } A \geqslant 0; \tag{13a}$$

$$\mathbf{T}_1 = \begin{bmatrix} e^{-\gamma_1(l_1/a_0)} & 0 \\ 0 & e^{-i\gamma_2(l_1/a_0)} \end{bmatrix}, \qquad \mathbf{T}_2 = \begin{bmatrix} e^{-\gamma_1(l_2/a_0)} & 0 \\ 0 & e^{-i\gamma_2(l_2/a_0)} \end{bmatrix}, \quad \text{for } A < 0. \tag{13b}$$

$\mathbf{r}_a$ and $\mathbf{r}_d$ are the reflection matrices of waves incident upon boundaries a and d, respectively:

$$\mathbf{r}_a = \mathbf{r}_d = \begin{bmatrix} \eta_1(i\gamma_1 + k_r) & \eta_2(\gamma_2 + k_r) \\ i(\gamma_1 - \eta_1) + k_t & (\gamma_2 - i\eta_2) + k_t \end{bmatrix}^{-1} \begin{bmatrix} -\eta_1(i\gamma_1 - k_r) & -\eta_2(\gamma_2 - k_r) \\ i(\gamma_1 - \eta_1) - k_t & (\gamma_2 - i\eta_2) - k_t \end{bmatrix},$$

$$\text{for } A \geqslant 0, \tag{14}$$

where

$$\eta_1 = \frac{\gamma_1^2 - \omega^2}{\gamma_1\left(1 + \varepsilon - \dfrac{\varepsilon}{\alpha}\right)}, \qquad \eta_2 = \frac{\gamma_2^2 + \omega^2}{i\gamma_2\left(1 + \varepsilon - \dfrac{\varepsilon}{\alpha}\right)}, \tag{14a, b}$$

and

$$\mathbf{r}_a = \mathbf{r}_d = \begin{bmatrix} \eta_1(\gamma_1 + k_r) & \eta_2(i\gamma_2 + k_r) \\ (\gamma_1 - i\eta_1) + k_t & i(\gamma_2 - \eta_2) + k_t \end{bmatrix}^{-1} \begin{bmatrix} -\eta_1(\gamma_1 - k_r) & -\eta_2(i\gamma_2 - k_r) \\ (\gamma_1 - i\eta_1) - k_t & i(\gamma_2 - \eta_2) - k_t \end{bmatrix},$$

$$\text{for } A < 0, \tag{15}$$

where

$$\eta_1 = \frac{\gamma_1^2 + \omega^2}{i\gamma_1\left(1 + \varepsilon - \dfrac{\varepsilon}{\alpha}\right)}, \qquad \eta_2 = \frac{\gamma_2^2 - \omega^2}{\gamma_2\left(1 + \varepsilon - \dfrac{\varepsilon}{\alpha}\right)}. \tag{15a, b}$$

$\mathbf{r}_{bc}$ and $\mathbf{t}_{bc}$ (listed in Appendix A for a general support) are the reflection and transmission matrices of incident waves upon the intermediate support, respectively. In the development of the above equations, $k_{ta} = k_{tbc} = k_{td} = k_t$ and $k_{ra} = k_{rbc} = k_{rd} = k_r$ are assumed throughout this paper.

Solving the above matrix equations gives

$$(\mathbf{r}_a \mathbf{T}_1 \mathbf{R}_b \mathbf{T}_1 - \mathbf{I})\mathbf{C}_a^+ = 0, \tag{16}$$

where $\mathbf{I}$ denotes the 2×2 identity matrix. For non-trivial solutions, the natural frequencies of the system are obtained from

$$C(\omega) = \text{Det}\,[(\mathbf{r}_a \mathbf{T}_1 \mathbf{R}_b \mathbf{T}_1 - \mathbf{I})] = 0. \tag{17}$$

Typical plots of $C(\omega)$ versus ω for the symmetric rotating shaft system ($l_1 = l_2$) are shown in Figure 2. Comparing Figures 2(a) and (b), it is seen that small incremental steps are required for finding the roots of $C(\omega)$ when the subsystems are weakly coupled through the intermediate support [see Figure 2(b)]. In Figure 2(b), two successive natural frequencies are closely spaced, indicating that they are in a veering zone. Moreover, both Re $[C(\omega)]$ and Im $[C(\omega)]$ experience sharp jumps near the natural frequencies, but the functions remain continuous and finite. Similar phenomenon also occurs when the span lengths are slightly different.

4. RESULTS AND DISCUSSION

Results for the first four eigensolutions are presented as functions of the system parameters: slenderness ratio (σ), support stiffness (k_t, k_r), rotation speed (β), and axial force (ε). Define the slenderness ratio σ and the span length disorder Δ as

$$\sigma = \frac{a_0}{l_1 + l_2}, \qquad \Delta = \frac{l_2 - l_1}{l_1 + l_2} \times 100\%. \tag{18a, b}$$

Table 1 summarizes the values of the system parameters used in the numerical studies. For each natural frequency, the corresponding mode shape and amplitude ratio (R) between the two sub-spans are found. The amplitude ratio is defined as

$$R = \begin{cases} \dfrac{|u_2|}{|u_1|}, & \text{for } |u_1| \geqslant |u_2|, \\ \dfrac{|u_1|}{|u_2|}, & \text{for } |u_1| < |u_2|, \end{cases} \tag{19}$$

TABLE 1

List of system parameters

a_0	0·0955 m*	
$l_1 + l_2$	1 m	
ρ	7700 kg/m^3	
K	0·9*	
E	207×10^9 N/m^2*	
G	$77{\cdot}7 \times 10^9$ N/m^2*	
K_{T0}	10^9 N/m^2†	$K_{Ta} = K_{Tbc} = K_{Td} = nK_{T0}$, $n = 1, 2, \ldots$
K_{R0}	10^9 N·m/rad†	$K_{Ra} = K_{Rbc} = K_{Rd} = nK_{R0}$, $n = 1, 2, \ldots$

* Reference [10].

† Typical bearing stiffness of turbo machinery, reference [30].

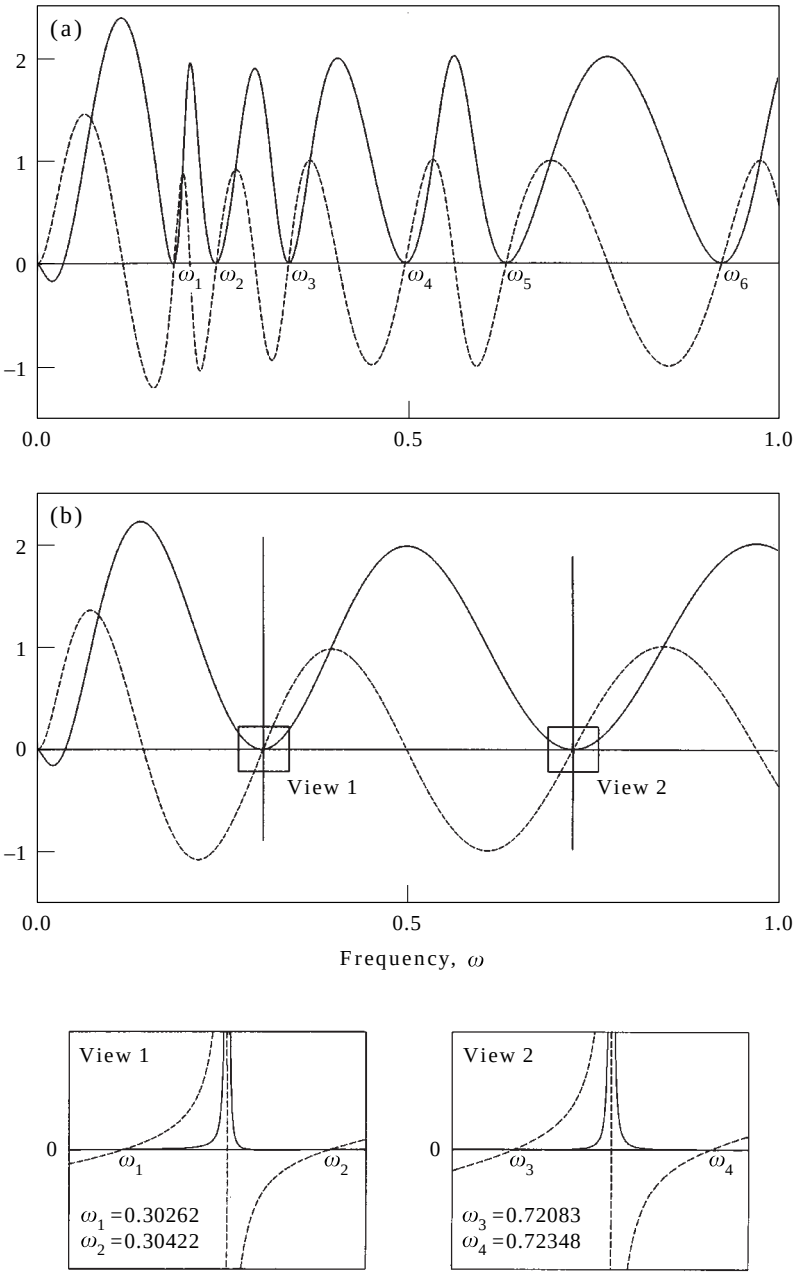

Figure 2. Typical plots of the characteristic equation of the forward precession mode of the rotating Timoshenko shaft system, $\alpha = 0{\cdot}3378$, $\beta = 0{\cdot}01$, $\varepsilon = 0$, $l_1 = l_2$; (a) $k_t = k_{t0}$, $k_r = k_{r0}$, (b) $k_t = \infty$, $k_r = 0$; Re $[C(\omega)]$ (——), Im $[C(\omega)]$ (– – –).

where u_1 and u_2 are the maximum displacements of the sub-spans. To study the effects of shear deformation on mode localization, results obtained for both the Timoshenko and Rayleigh shaft models (which hereafter, for brevity, are denoted by TM and RM, respectively) are compared in terms of their amplitude ratios.

Since the quantitative definition of mode localization is subjective and relative depending on the types of applications, the term *localized mode* in this paper refers to any mode which has a non-zero ratio of span length disorder to amplitude ratio and with *sufficiently small* span length disorder. Based on this definition, even a mode with $\Delta/R \approx \Delta$ might be considered localized. However, in such a case, the term *weakly localized* is used instead of *not localized*. In the numerical studies, Δ is chosen to be 2% which satisfies our definition of localization. For brevity, the term mode localization increases (decreases) means that the degree of mode localization Δ/R increases (decreases) as R decreases (increases) for a fixed Δ.

As a general note, the discussion on the effects of system parameters on mode localization in sections 4.1 to 4.4 for finite k_t cannot be generalized to results when the stiffness is *very* large. In the latter case, the dynamic behaviour of the rotating shaft becomes different (refer to section 4.5) and follows that of a mono-coupled system with the sub-spans coupled only by the rotational spring.

4.1. EFFECTS OF SHEAR DEFORMATION

The effects of shear on mode localization is investigated in terms of the slenderness ratio σ. As σ or the mode number increases, the shear deformation effects become more dominant, and the TM gives a more accurate prediction of the system response. Figure 3 shows the effects of σ on mode localization by comparing the amplitude ratio R for both TM and RM. Note that the data points are discretely jointed. Representative mode shapes are also plotted.

Results show that both shaft models exhibit similar qualitative behavior in mode localization. The modes are strongly localized for small values of σ, and the localization in general decreases with increasing σ. Modes of TM are more localized than those of RM. As the slenderness ratio and/or mode number increases, the difference in R between the two models becomes larger. This indicates that the effects of shear on mode localization are important for rotating shafts with large σ and for higher modes. As noted before, these trends are generally valid when the transverse spring stiffness is not very large. In Figures 5 and 6 of reference [27], it is shown that for a non-rotating beam with $k_t = \infty$, mode localization increases with σ and the mode number.

4.2. EFFECTS OF SUPPORT STIFFNESS

Previous research on mode localization has focused on mono-coupled systems in which the coupling between the subsystems is usually modelled by a simple support and a rotational spring [18]. However, in practical applications, infinite stiffness for the transverse displacement does not exist. The system studied in this paper represents a rotating shaft on bearing supports (K_{T0} and K_{R0} are typical bearing values in turbo machinery; see Table 1). This section investigates the combined effects of transverse and rotational support stiffness on mode localization.

Figure 4 plots the amplitude ratio as a function of transverse spring stiffness for four different rotational spring stiffness. In general, as the mode number increases, differences in R between the RM and TM become larger. It is also seen

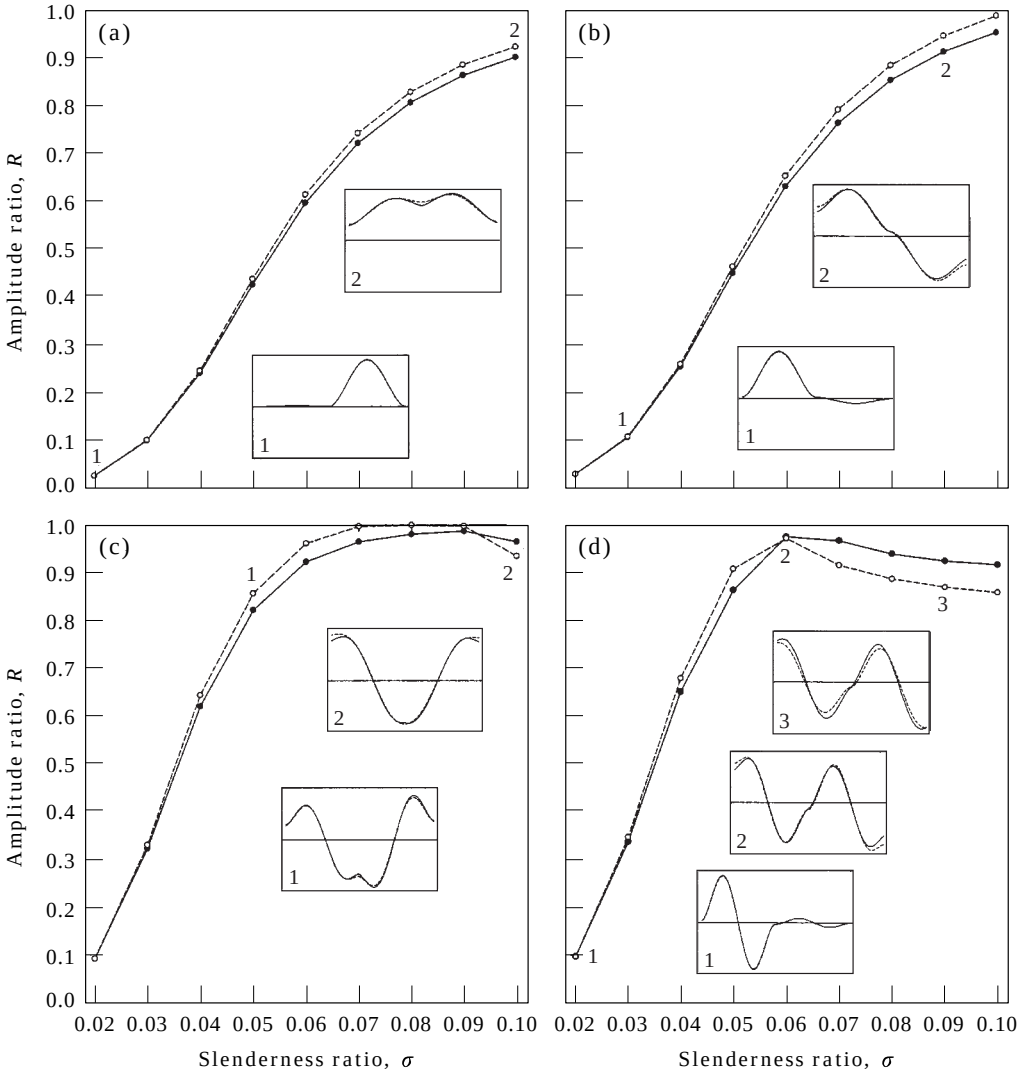

Figure 3. Amplitude ratio R as a function of slenderness ratio σ for the forward precession mode, $\alpha = 0{\cdot}3378$, $\beta = 0{\cdot}01$, $\varepsilon = 0$, $\Delta = 2\%$, $k_t = k_{t0}$, $k_r = k_{r0}$; (a) 1st, (b) 2nd, (c) 3rd, (d) 4th mode; TM (●), RM (○). Representative modeshapes are shown; TM (——), RM (– – –).

that the effects on localization are significantly different between the $k_r \neq 0$ and $k_r = 0$ cases. When $k_r \neq 0$, mode localization increases with the transverse stiffness, agreeing with a well known observation that the weaker the inter-span coupling, the stronger is the localization [18]. Moreover, localization has a weaker dependence on the rotational spring stiffness. The amplitude ratios for the $k_r = k_{r0}$ and $k_r = 10k_{r0}$ cases differ by at most 20% over the range of k_t, and comparing the $k_r = 10k_{r0}$ and $k_r = 50k_{r0}$ cases, there is practically no difference. This dependence, however, increases with the mode number and k_t. The results here show that the transverse span support stiffness is a much more important factor than the rotational stiffness in determining the amount of mode localization.

When $k_r = 0$, the dependence of R on k_t is not monotonic. It is seen that localization in the first and second modes is strongest when $k_t = k_{t0}$, and in the third and fourth modes it is strongest when $k_t = 5k_{t0}$. Hence, when the intermediate support consists of only a transverse spring, mode localization does not always increase when the inter-span coupling becomes weaker. This is true for both the TM and RM. To understand this phenomenon, consider the wave propagation at the support. Figure 5 plots the frequency dependence of a vibration ratio δ [31]

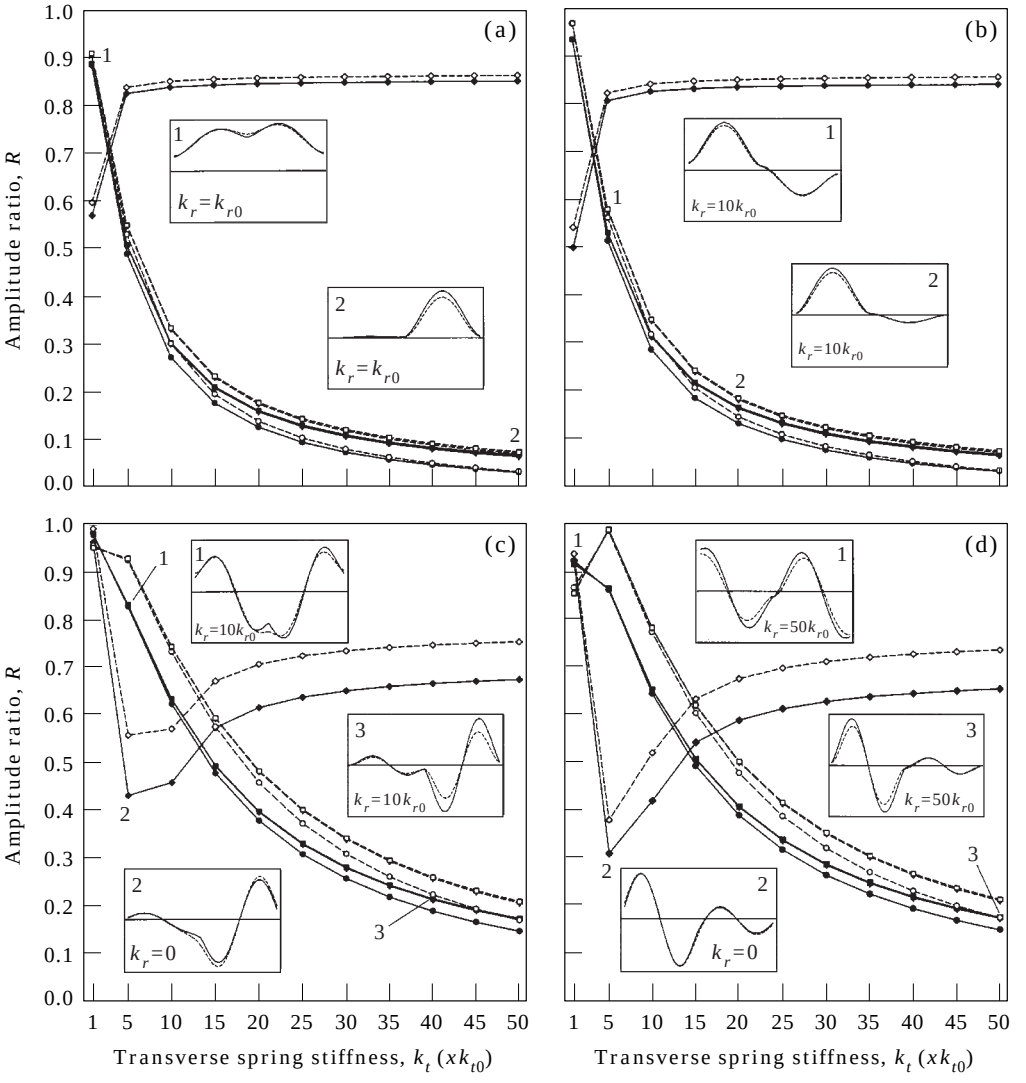

Figure 4. Amplitude ratio R as a function of transverse spring stiffness for forward precession mode, $\alpha = 0{\cdot}3378$, $\beta = 0{\cdot}01$, $\varepsilon = 0$, $\Delta = 2\%$; (a) 1st, (b) 2nd, (c) 3rd, (d) 4th mode; TM (●), RM (○) for $k_r = k_{r0}$; TM (▼), RM (▽) for $k_r = 10k_{r0}$; TM (■), RM (□) for $k_r = 50k_{r0}$; TM (◆), RM (◇) for $k_r = 0$. Representative modeshapes are shown; TM (——), RM (– – –).

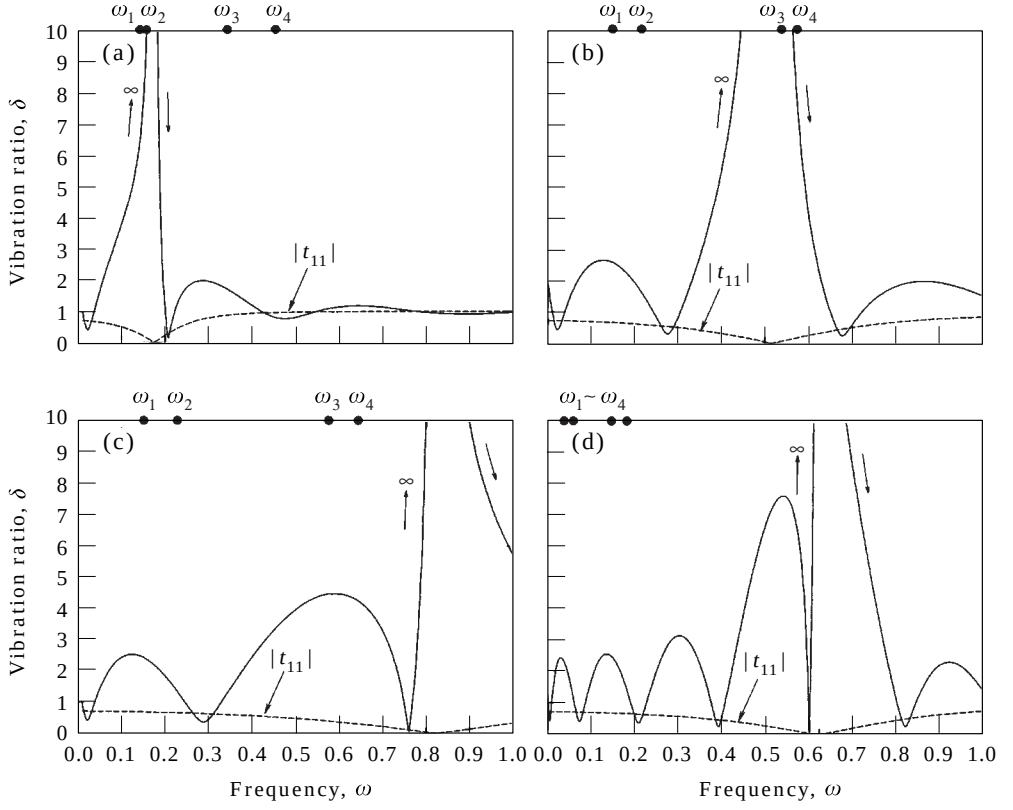

Figure 5. Vibration ratio δ as a function of frequency ω for the Rayleigh model, $\alpha = 0{\cdot}3378$, $\beta = 0{\cdot}01$, $\varepsilon = 0$, $\Delta = 2\%$, $k_r = 0$; (a) $k_t = k_{t0}$, (b) $k_t = 5k_{t0}$, (c) $k_t = 10k_{t0}$, (d) $k_t = 50k_{t0}$. Dashed curve (– – –) shows the modulus of the transmission coefficient of the propagating wave (t_{11}) at the support. Natural frequencies are marked by dots (●) on the upper frequency axis.

and the wave transmission coefficient (t_{11}) for the RM. δ is the ratio of the amplitudes of propagating waves on both sides of the support and is defined as

$$\delta = \frac{\sqrt{1 + r^2 - 2r\cos\psi_a}}{t}, \qquad \psi_a = \phi_a + \phi_r + \phi_t \pm \frac{\pi}{2} - 2\gamma_1 l_1, \tag{20}$$

where $r = |r_{11}|$, $t = |t_{11}|$, $\phi_a = \arg(r_a)$, r_a is r_{11} at the left boundary, $\phi_r = \arg(r_{11})$, $\phi_t = \arg(t_{11})$. It is noted that $\delta \neq R$ since attenuating waves are neglected in δ. Nevertheless, they show the same qualitative trends [26, 32]. The natural frequencies ω_j of the system are also marked (symbol ●) on the frequency axis. When $\delta \approx 1$, mode localization is very weak. From equation (20) and also shown in the plots of Figure 5, δ becomes unbounded when t approaches zero. The frequency at which $t_{11} = 0$ is the impedance mismatching frequency ω_{imm}. Figure 5(a) shows the result for $k_t = k_{t0}$. It is seen that both ω_1 and ω_2 are close to ω_{imm}, and thus the first and second modes experience the strongest localization at $k_t = k_{t0}$. Similar reasoning can be applied to Figure 5(b). Note that ω_{imm} can be solved directly from the condition $t_{11} = 0$ or

$$2\gamma_2(\gamma_1^2 + \gamma_2^2) = k_t. \tag{21}$$

The analytical solution of the above equation shows that ω_{imm} increases rapidly as k_t is increased. This is depicted in Figures 5(c, d) which also show that the increase of ω_j is limited by the eigenvalue inclusion principle [33]. Thus, for large k_t, strongest localization occurs at much higher modes.

4.3. EFFECTS OF ROTATION SPEED

It is well known that rotating shafts have forward precession and backward precession modes with different natural frequencies. The mode shapes associated with these two precession modes are generally different except for the hinged

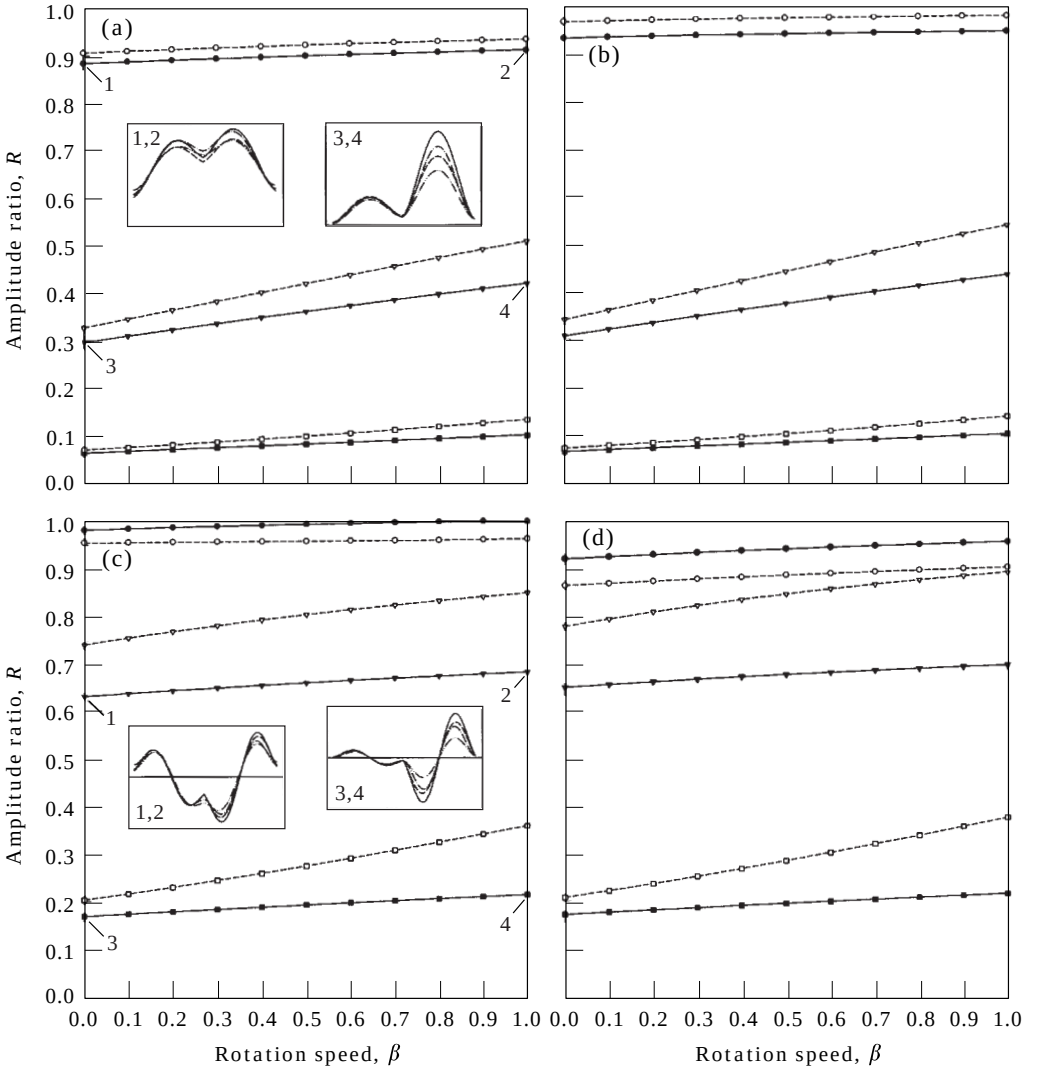

Figure 6. Amplitude ratio R as a function of rotational speed β, $\alpha = 0{\cdot}3378$, $\varepsilon = 0$, $\Delta = 2\%$; (a) 1st, (b) 2nd, (c) 3rd, (d) 4th mode; TM (●), RM (○) for $k_t = k_{t0}$, $k_r = k_{r0}$; TM (▼), RM (▽) for $k_t = 10k_{t0}$, $k_r = 10k_{r0}$; TM (■), RM (□) for $k_t = 50k_{t0}$, $k_r = 50k_{r0}$. Representative modeshapes are shown; TM (——), RM (–·–) for $\beta = 0$; TM (– – –), RM (–··–) for $\beta = 1$.

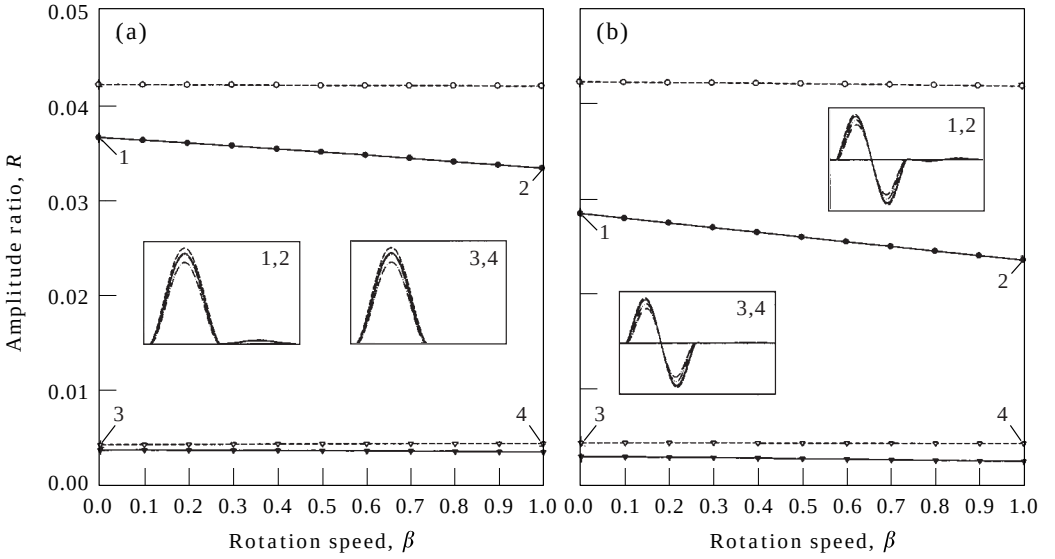

Figure 7. Amplitude ratio R as a function of rotational speed β when $k_t = \infty$, $\alpha = 0{\cdot}3378$, $\varepsilon = 0$, $\Delta = 2\%$; (a) 2nd, (b) 4th mode; TM (●), RM (○) for $k_r = k_{r0}$; TM (▼), RM (▽) for $k_r = 10k_{r0}$. Representative modeshapes are shown; TM (——), RM (–·–) for $\beta = 0$; TM (– – –), RM (–··–) for $\beta = 1$.

boundary condition [2]. Figure 6 shows R as a function of the rotation speed for the forward precession mode under various support conditions. Results for the second and fourth modes when $k_t = \infty$ are shown in Figure 7. It is seen that, for k_t finite, mode localization decreases with β, while for $k_t = \infty$, it increases with β. Figure 6 also shows that for bi-coupled systems, the effects of the rotation speed are more pronounced when the modes are strongly localized. However, it should be pointed out that in the practical range of the rotation speed ($\beta = 0{\cdot}1 \approx 9 \times 10^4$ rpm), the effects of speed on mode localization are basically insignificant. Comparison of results shown in Figures 6 and 7 reveals that the effects of rotation speed are more pronounced for the RM in the finite stiffness cases, but more for the TM in the $k_t = \infty$ cases.

Figure 8 shows R as a function of the rotation speed for the backward precession mode under different support conditions. Results for the second and fourth modes when $k_t = \infty$ are shown in Figures 8(e) and 8(f), respectively. In general, for a given β, the backward precession modes are more localized than the forward precession modes. The effects of the rotation speed on the mode localization are significant for both the RM and TM, and unlike the forward precession modes, the trends do not constitute a pattern. In the second and fourth modes of Figures 8(e) and (f), a mode delocalization phenomenon [27, 32] is observed in which the localization first decreases and then increases as the rotation speed is increased.

4.4. EFFECTS OF AXIAL LOADS

Figures 9 and 10 show the effects of axial loads, both tension and compression, on the mode localization. Results shown in Figure 9 are for the cases with finite

support stiffness, and results for the second and fourth modes when $k_t = \infty$ are plotted in Figure 10. The range of loads applied is $\varepsilon = -0{\cdot}05 \sim 0{\cdot}05$, where the maximum compressive load is chosen to be smaller than the first buckling load to ensure that ω_1 is real. For example, $\omega_1 = 0{\cdot}1433$ at $\varepsilon = -0{\cdot}05$ when $\beta = 0{\cdot}01$, $k_t = k_{t0}$ and $k_r = k_{r0}$ (weakest constraint case presented).

Results of Figure 9 show that, when k_t is finite, mode localization decreases with increasing tension and increases with increasing compression. On the other hand, when $k_t = \infty$, the trends of the effects reverse. Moreover, Figure 9 shows that for

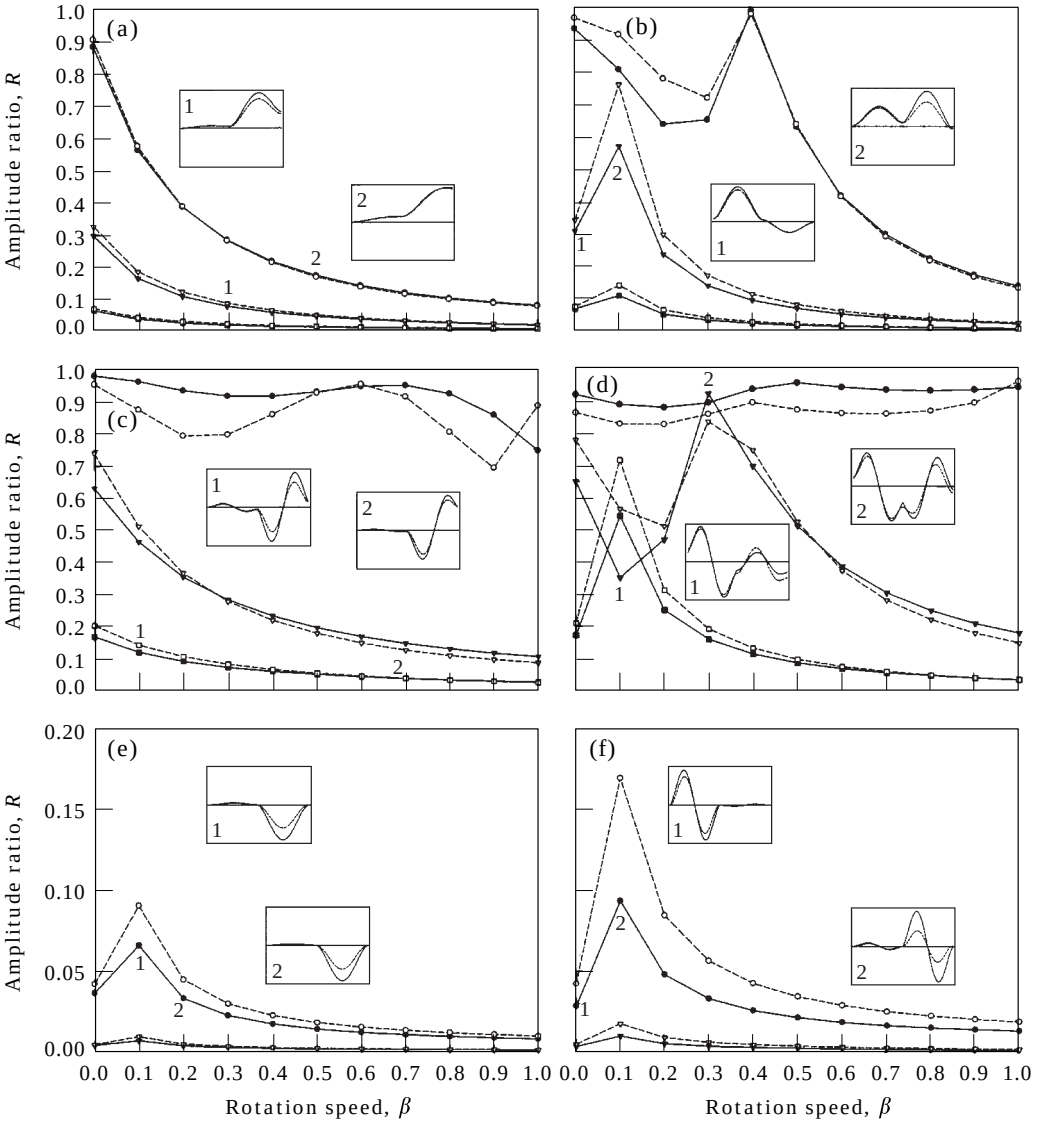

Figure 8. Amplitude ratio R as a function of rotational speed β, $\alpha = 0{\cdot}3378$, $\varepsilon = 0$, $\Delta = 2\%$; (a) 1st, (b) 2nd, (c) 3rd, (d) 4th, (e) 2nd, (f) 4th mode. For (a)–(d), TM (●), RM (○) for $k_t = k_{t0}$, $k_r = k_{r0}$; TM (▼), RM (▽) for $k_t = 10k_{t0}$, $k_r = 10k_{r0}$; TM (■), RM (□) for $k_t = 50k_{t0}$, $k_r = 50k_{r0}$. For (e)–(f), TM (●), RM (○) for $k_t = \infty$, $k_r = k_{r0}$; TM (▼), RM (▽) for $k_t = \infty$, $k_r = 10k_{r0}$.

bi-coupled systems, the effects of the axial strain are more pronounced when the modes are strongly localized. It was mentioned by Lust *et al*. [27] that for a two-span Timoshenko beam, an application of a compressive load can lead to a slight delocalizing effect when $k_t = \infty$ (mono-coupled system). This phenomenon is confirmed by our results in the second and fourth modes shown in Figure 10. Comparison of plots in Figure 9 indicates that the RM and TM have similar qualitative behaviour under the action of axial loads when the spring stiffness is finite. However, when $k_t = \infty$, mode localization in the RM appears to be unaffected by changes in the axial load, as shown in Figure 10.

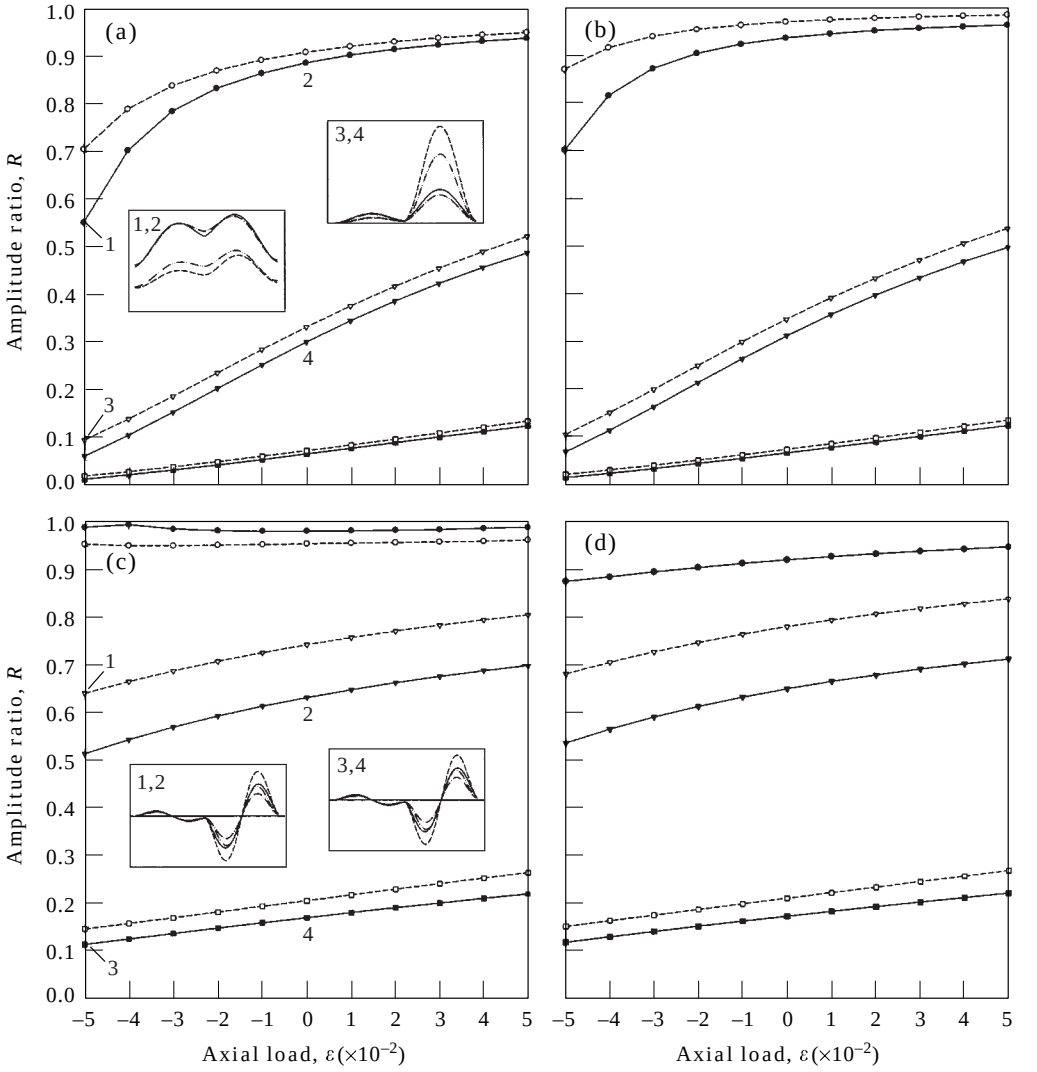

Figure 9. Amplitude ratio R as a function of axial load ε, $\alpha = 0{\cdot}3378$, $\beta = 0{\cdot}01$, $\Delta = 2\%$; (a) 1st, (b) 2nd, (c) 3rd, (d) 4th mode; TM (●), RM (○) for $k_t = k_{t0}$, $k_r = k_{r0}$; TM (▼), RM (▽) for $k_t = 10k_{t0}$, $k_r = 10k_{r0}$; TM (■), RM (□) for $k_t = 50k_{t0}$, $k_r = 50k_{r0}$. Representative modeshapes are shown; TM (——), RM (–·–) for $\varepsilon = 0$; TM (– – –), RM (–··–) for $\varepsilon = -0{\cdot}05$.

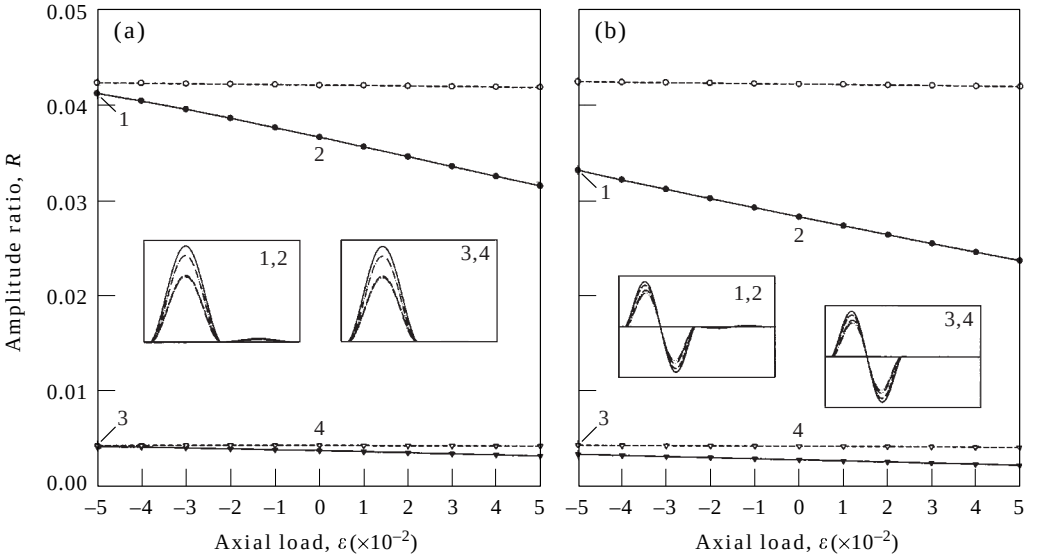

Figure 10. Amplitude ratio R as a function of axial load ε, $\alpha = 0{\cdot}3378$, $\beta = 0{\cdot}01$, $\Delta = 2\%$; (a) 2nd, (b) 4th mode; TM (●), RM (○) for $k_r = k_{r0}$; TM (▼), RM (▽) for $k_r = 10k_{r0}$. Representative modeshapes are shown; TM (——), RM (–·–) for $\varepsilon = 0$; TM (– – –), RM (–··–) for $\varepsilon = -0{\cdot}05$.

4.5. COMMENTS ON THE MODELLING OF THE SPAN SUPPORT

In the study of mode localization in elastic beams on regularly spaced supports, it is common to model the support as a mono-coupling constraint of a simple support ($k_t = \infty$) and a rotational spring [18]. However, it may be more realistic for certain applications to model the support as a combination of transverse and rotational springs with finite stiffness such that adjacent sub-spans are bi-coupled and vibration energy is transferred through the two degrees of motion. Moreover, our results have clearly indicated significant differences in the dynamic behaviour of the rotating shaft system between finite and infinite stiffness cases. Thus the issue of modelling of the span support is important in the study of mode localization. Table 2 provides an overview of the differences in the effects of systems parameters on the localization trends for the mono-coupled ($k_t = \infty$, k_r finite) and bi-coupled (k_t, k_r finite) systems.

In addition to the results presented in sections 4.1 to 4.4, two other support conditions should be mentioned in order to give a complete picture of the localization patterns. Figure 11 shows the amplitude ratios (log scale) of the second and fourth forward precession modes as a function of the rotational spring stiffness for a bi-coupled TM system. The results for the mono-coupled system ($k_t = \infty$ case) are also plotted for comparison. In the latter case, localization increases as the rotational spring stiffness is increased or when the coupling between spans becomes weaker. This is the classical result. However, for very large transverse stiffness (say $k_r = 5000k_{t0}$), the change in R follows the trend of the mono-coupled system up to a certain value of k_r, beyond which the system behaves as a bi-coupled system. For the second mode, R decreases up to $k_r \approx 50k_{r0}$ and then increases with increasing k_r. Thus, when the transverse support stiffness is

TABLE 2

Summary of the effects of system parameters on the mode localization for two models of the span support

System parameters	Support model and coupling type: mono-coupled 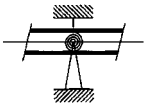	Support model and coupling type: bi-coupled 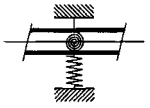	Range of parameters considered in the analyses
Slenderness ratio, σ	⇑	⇓	$0{\cdot}02 \leqslant \sigma \leqslant 0{\cdot}1$
Mode number	⇑	⇓	Shown up to the fourth mode
Translational spring stiffness, k_t	⇑	⇑	See Figure 4
Rotational spring stiffness, k_r	⇑	⇓	See Figure 4
Rotational speed, β (forward precession)	⇑	⇓	$0 \leqslant \beta \leqslant 1$
Axial compression, $-\varepsilon$	⇓	⇑	$0 \leqslant -\varepsilon \leqslant 0{\cdot}05 \leqslant \varepsilon_{\text{critical load}}$
Axial tension, $+\varepsilon$	⇑	⇓	$0 \leqslant \varepsilon \leqslant 0{\cdot}05$

⇑ degree of mode localization increases as the parameter in the first column increases.
⇓ degree of mode localization decreases as the parameter in the first column increases.
Note: Also refer to two exceptional cases of the bi-coupled system in section 4.5.

very large, the system may be treated as mono-coupled for small k_r, but must be treated as bi-coupled when k_r is sufficiently large. For large, k_r, R approaches a constant, indicating again the weak dependence of localization on the rotational span support stiffness in bi-coupled systems.

The case of a bi-coupled system with $k_r = 0$ is discussed in section 4.2 and the impedance mismatching frequency ω_{imm} is defined. When the rotational spring support is present, the wave propagation changes from the impedance mismatching to a matching phenomenon [13] in which the reflection coefficient r_{11} can become zero. Define the impedance matching frequency ω_{im} as the frequency at which $r_{11} = 0$. It was shown that, for an Euler–Bernoulli beam, when a natural frequency is close to ω_{im}, the corresponding mode is delocalized since vibration energy is easily transmitted [26]. In relation to the vibration ratio δ, when $\omega_j \approx \omega_{im}$,

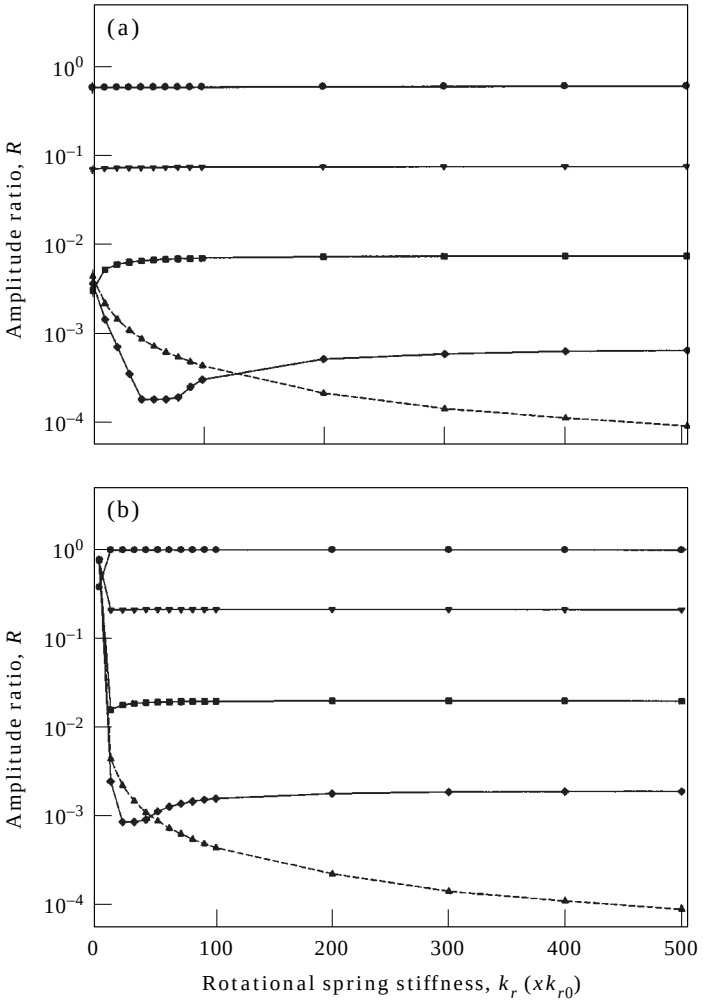

Figure 11. Amplitude ratio R as a function of rotational spring stiffness for the forward precession modes of TM, $\alpha = 0{\cdot}3378$, $\beta = 0{\cdot}01$, $\varepsilon = 0$, $\Delta = 2\%$; (a) 2nd, (b) 4th mode; $k_t = 50k_{t0}$ (●), $k_t = 50k_{t0}$ (▼), $k_t = 500k_{t0}$ (■), $k_t = 5000k_{t0}$ (◆), $k_t = \infty$ (▲).

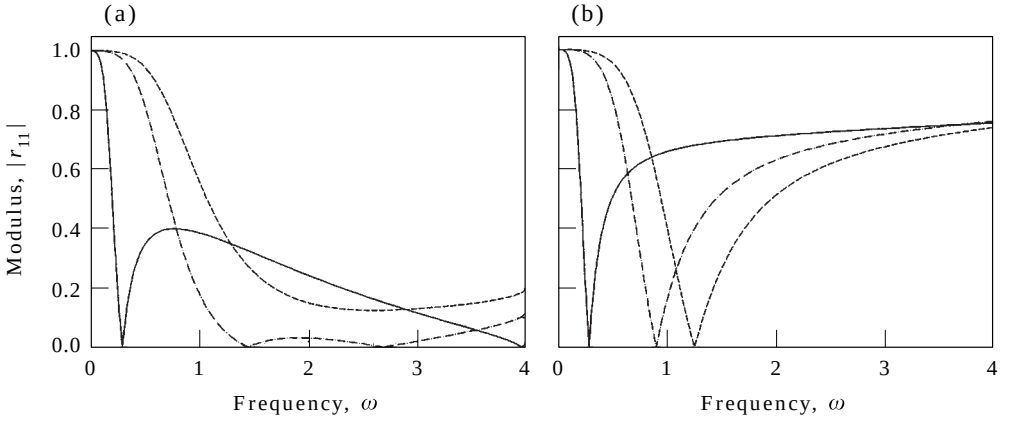

Figure 12. The reflection coefficient of the propagating wave (r_{11}) at the support for forward precession modes of (a) TM and (b) RM, $\alpha = 0{\cdot}3378$, $\beta = 0{\cdot}01$, $\varepsilon = 0$; $k_t = k_{t0}$ and $k_r = k_{r0}$ (——), $k_t = 6k_{t0}$ and $k_r = 6k_{r0}$ (–·–), $k_t = 10k_{t0}$ and $k_r = 10k_{r0}$ (– – –). Impedance matching frequencies occur when $r_{11} = 0$.

the jth mode becomes weakly localized and $\delta \approx 1$. Possible support conditions for which the delocalization can occur were also discussed in reference [26]. It should be noted that while there is only one real root for ω_{im} in both the Euler–Bernoulli model [26] and the RM [see Figure 12(b)], the TM can have more than one root. Figure 12(a) plots the wave reflection coefficient of the rotating shaft as a function of frequency for three different support conditions. The three cases have either two roots, one root, or no root. Based on Figure 12, it is thus possible for the rotating shaft system (both RM and TM) to experience mode delocalization due to impedance matching. Lust *et al*. [27] also reported a delocalization in Timoshenko beams and attributed three factors to that occurrence. Note that, in contrast, there is always one real root for ω_{imm} in both the RM and TM.

5. SUMMARY AND CONCLUSIONS

A numerical study is performed to investigate the mode localization in a dual-span rotating shaft on regularly spaced bearing supports by introducing a small disorder in the span length. The shaft is modelled as a rotating Timoshenko beam subject to axial loads and its free response is evaluated by the phase closure principle. The main findings of this work are as follows.

(1) The issue of modelling of the span support is important in the study of mode localization. It is shown that significant differences exist between results for the mono-coupled (simple support with finite rotational spring stiffness) and the bi-coupled (finite transverse and rotational spring stiffness) systems. When the transverse support stiffness is very large, the system may be treated as mono-coupled for small rotational spring stiffness, but must be treated as bi-coupled when the rotational stiffness is sufficiently large.

(2) For mono-coupled systems ($k_t = \infty$ and k_r finite, or k_t finite and $k_r = \infty$), the degree of mode localization increases monotonically with the support spring

stiffness, as the strength of the inter-span coupling is weakened. In general, the transverse support stiffness is a more important factor than the rotational stiffness in determining the amount of mode localization. The degree of localization depends weakly on the rotational spring stiffness except when the support has a very large transverse spring stiffness.

(3) When the span support consists of only a transverse spring (i.e., strongly coupled in rotation), mode localization does not always increase when the inter-span coupling strength is decreased. This can be explained by the impedance mismatching of the wave propagation at some particular modes. However, when the support is constrained by both the transverse and rotational springs, wave impedance matching occurs at some frequencies allowing energy to be transmitted easily and mode delocalization is possible for both the Rayleigh and Timoshenko models.

(4) In the practical range of rotational speed, mode localization of the forward precession modes is slightly affected by changes in the speed. However, the effects of rotation speed are significant for the backward precession modes.

(5) For bi-coupled systems, mode localization decreases with increasing tension and increases with increasing compressive load. On the other hand, for mono-coupled systems (simple support with finite rotational spring stiffness), the trend of these effects reverse.

(6) The qualitative behaviour of mode localization is found to be similar for both the Rayleigh and Timoshenko models. As the slenderness ratio increases, the difference in mode localization between these two models becomes larger. In general, localization is stronger in the Timoshenko model. For mono-coupled systems, mode localization in the Rayleigh model is slightly affected by changes in either the rotation speed or the axial load.

ACKNOWLEDGMENT

The authors would like to acknowledge the support of the National Science Foundation and the Institute for Manufacturing Research of Wayne State University for this research work.

REFERENCES

1. T. C. Huang 1961 *ASME Journal of Applied Mechanics* **28**, 579–584. The effect of rotary inertia and of shear deformation on the frequency and normal mode equations of uniform beams with simple end conditions.
2. C. W. Lee 1993 *Vibration Analysis of Rotors*. Amsterdam: Kluwer Academic.
3. F. M. Dimentberg 1961 *Flexural Vibrations of Rotating Shafts*. London: Butterworth.
4. A. D. Dimarogonas and S. A. Paipeties 1983 *Analytical Method in Rotor Dynamics*. New York: Applied Science.
5. J. S. Rao 1983 *Rotor Dynamics*. New York: Wiley.
6. L. W. Chen and H. K. Chen 1995 *American Institute of Aeronautics and Astronautics Journal* **39**(9), 1569–1573. Whirl speeds and stability of rotating shaft subjected to end loads.

7. K. W. Wang, Y. C. Shin and C. H. Chen 1991 *Proceedings of Institution of Mechanical Engineers* **205**, 147–154. On the natural frequencies of high-speed spindles with angular contact bearings.
8. T. C. Huang and F. C. C. Huang 1967 *ASME Journal of Engineering for Industry* **89**, 713–718. On precession and critical speeds for two-bearing machines with overhang weight.
9. S. H. Choi, C. Pierre and A. G. Ulsoy 1992 *ASME Journal of Vibration and Acoustics* **114**, 249–259. Consistent modeling of rotating Timoshenko shafts subject to axial loads.
10. R. Katz, C. W. Lee, A. G. Ulsoy and R. A. Scott 1988 *Journal of Sound and Vibration* **122**, 131–148. The dynamic response of a rotating shaft subject to a moving load.
11. R. P. S. Han and J. W.-Z. Zu 1992 *Journal of Sound and Vibration* **156**, 1–16. Modal analysis of rotating shafts: a body-fixed axis formulation approach.
12. C. A. Tan and W. Kuang 1995 *Journal of Sound and Vibration* **183**, 451–474. Vibration of a rotating discontinuous shaft by the distributed transfer function method.
13. C. A. Tan and B. Kang 1998 *Journal of Sound and Vibration* **213**(3), 483–510. Wave reflection and transmission in an axially strained, rotating Timoshenko shaft.
14. C. H. Hodges 1982 *Journal of Sound and Vibration* **82**(3), 411–424. Confinement of vibration by structural irregularity.
15. C. H. Hodges and J. Woodhouse 1983 *Journal of the Acoustical Society of America* **74**, 894–905. Vibration isolation from irregularity in a nearly periodic structure: theory and measurements.
16. N. A. Valero and O. O. Bendiksen 1986 *ASME Journal of Engineering for Gas Turbines and Power* **108**(4), 293–299. Vibration characteristics of mistuned shrouded blade assemblies.
17. O. O. Bendiksen 1987 *American Institute of Aeronautics and Astronautics Journal* **25**(9), 1241–1248. Mode localization phenomena in large space structures.
18. C. Pierre, D. M. Tang and E. H. Dowell 1987 *American Institute of Aeronautics and Astronautics Journal* **25**(9), 1249–1257. Localized vibrations of disordered multispan beams: theory and experiment.
19. C. Pierre 1988 *Journal of Sound and Vibration* **126**(3), 485–502. Mode localization and eigenvalue loci veering phenomena in disordered structures.
20. P. T. Chen and J. H. Ginsberg 1992 *ASME Journal of Vibration and Acoustics* **114**, 141–148. On the relationship between veering of eigenvalue loci and parameter sensitivity of eigenfunctions.
21. A. G. Ulsoy, C. Pierre and S. H. Choi 1995 *ASME Proceedings of the* 1995 *Design Engineering Technical Conferences* **3**(C), 105–116. Vibration localization in rotating shafts, Part I: theory.
22. A. G. Ulsoy, C. Pierre and S. H. Choi 1995 *ASME Proceedings of the* 1995 *Design Engineering Technical Conferences* **3**(C), 117–124. Vibration localization in rotating shafts, Part II: experiment.
23. A. A. N. Al-Jawi, A. G. Ulsoy and C. Pierre 1995 *Journal of Sound and Vibration* **179**(2), 289–312. Vibration localization in band-wheel systems: theory and experiment.
24. A. A. N. Al-Jawi, C. Pierre and A. G. Ulsoy 1995 *Journal of Sound and Vibration* **179**(2), 243–266. Vibration localization in dual-span axially moving beams, Part I: formulation and results.
25. A. A. N. Al-Jawi, C. Pierre and A. G. Ulsoy 1995 *Journal of Sound and Vibration* **179**(2), 243–266. Vibration localization in dual-span axially moving beams, Part II: perturbation analysis.
26. C. H. Riedel and C. A. Tan 1998 *Journal of Sound and Vibration* **215**(3), 455–473. Dynamic characteristics and mode localization of elastically constrained axially moving strings and beams.

27. S. D. Lust, P. P. Friedmann and O. O. Bendiksen 1993 *American Institute of Aeronautics and Astronautics Journal* **31**(2), 348–355. Mode localization in multispan beams.
28. L. Cremer, M. Heckl and E. E. Ungar 1973 *Structure-Borne Sound*. Berlin: Springer.
29. D. J. Mead 1994 *Journal of Sound and Vibration* **171**, 695–702. Waves and modes in finite beams: application of the phase-closure principle.
30. F. F. Ehrich 1992 *Handbook of Rotordynamics*. New York: McGraw-Hill.
31. R. S. Langley 1995 *Journal of Sound and Vibration* **185**(1), 79–91. Mode localization up to high frequencies in coupled one-dimensional subsystems.
32. C. H. Riedel and C. A. Tan 1997 *ASME Proceedings of the ASME Design Engineering Technical Conference*. Paper DETC97/VB-3951, 14–17 September, Sacramento, CA. Mode localization and delocalization in constrained string and beams.
33. J. W. S. Rayleigh 1945 *The Theory of Sound*, Vol. I. New York: Dover.

APPENDIX A: REFLECTION AND TRANSMISSION MATRICES

When a set of waves are incident upon a point support consisting of transverse and rotational springs (k_1 and k_r, respectively), dampers (c_t and c_r, respectively), and a rotor mass m (with mass moment of inertia J_m), the wave reflection and transmission matrices at the support for a Timoshenko beam model are

$$\mathbf{r} = \frac{1}{D}\begin{bmatrix} r_{11} & r_{12} \\ r_{21} & r_{22} \end{bmatrix} \quad \text{and} \quad \mathbf{t} = \frac{1}{D}\begin{bmatrix} t_{11} & t_{12} \\ t_{21} & t_{22} \end{bmatrix},$$

where, for $A \geqslant 0$

$$\begin{aligned}
D &= \{\eta_1(2\gamma_1 - \mathrm{i}H_m) + \mathrm{i}\eta_2(2\gamma_1 + H_m)\}\{2\eta_1\gamma_2 - 2\mathrm{i}\eta_2\gamma_1 + H_s(\eta_1 - \eta_2)\},\\
r_{11} &= -2\eta_1\eta_2\gamma_1(H_m - H_s) + \mathrm{i}\eta_2^2 H_s(2\gamma_2 + H_m) - \mathrm{i}\eta_1^2 H_m(2\gamma_2 + H_s),\\
r_{12} &= -2\eta_2[\mathrm{i}\eta_1\{\gamma_2 H_m + H_s(\mathrm{i}\gamma_1 + H_m)\} + \eta_2\{\gamma_1 H_m - \mathrm{i}H_s(\gamma_2 + H_m)\}],\\
r_{21} &= 2\eta_1[\mathrm{i}\eta_1\{\gamma_2 H_m + H_s(\mathrm{i}\gamma_1 + H_m)\} + \eta_2\{\gamma_1 H_m - \mathrm{i}H_s(\gamma_2 + H_m)\}],\\
r_{22} &= 2\mathrm{i}\eta_1\eta_2\gamma_2(H_m - H_s) + \eta_2^2 H_m(2\gamma_1 - \mathrm{i}H_s) + \eta_1^2 H_s(\mathrm{i}H_m - 2\gamma_1),\\
t_{11} &= 2\eta_2^2\gamma_1(2\gamma_2 + H_m) + 2\eta_1^2\gamma_1(2\gamma_2 + H_s) - 2\mathrm{i}\eta_1\eta_2\{2\gamma_1^2 - \gamma_2(2\gamma_2 + H_m + H_s)\},\\
t_{12} &= 2\eta_2(\eta_2\gamma_1 H_m + \mathrm{i}\eta_1\gamma_2 H_m + \eta_1\gamma_1 H_s + \mathrm{i}\eta_2\gamma_2 H_s),\\
t_{21} &= -2\eta_1(\eta_2\gamma_1 H_m + \mathrm{i}\eta_1\gamma_2 H_m + \eta_1\gamma_1 H_s + \mathrm{i}\eta_2\gamma_2 H_s),\\
t_{22} &= 2\eta_1^2\gamma_2(2\gamma_1 - \mathrm{i}H_m) + 2\eta_2^2\gamma_2(2\gamma_1 - \mathrm{i}H_s) + 2\eta_1\eta_2\{2\mathrm{i}\gamma_2^2 - \mathrm{i}\gamma_1^2 - \gamma_1(H_m + H_s)\},\\
H_m &= k_r + \mathrm{i}c_r\omega - J_m\omega^2, \quad \text{and} \quad H_s = k_t + \mathrm{i}c_t\omega - m\omega^2,
\end{aligned}$$

and, for $A < 0$

r and **t** can be obtained by replacing $\mathrm{i}\gamma_1$ and γ_2 in the above expressions with γ_1 and $\mathrm{i}\gamma_2$, respectively. In this case, note that η_1 and η_2 are given by equations (15a, b).

Note that, for convenience, overbars for non-dimensional quantities have been dropped in the above expressions. For the system shown in Figure 1, $\mathbf{r}_{bc}$ and $\mathbf{t}_{bc}$ can be obtained by setting $c_t = c_r = m = J_m = 0$. Detailed derivations of **r** and **t** can be found in reference [13].